ACS OMEGA

Article

Cite This: ACS Omega 2019, 4, 8290−8298

http://pubs.acs.org/journal/acsodf

# Probing the Formation of Reactive Oxygen Species by a Porous Self-Assembled Benzophenone Bis-Urea Host

Baillie A. DeHaven,[†] Hannah K. Liberatore,[†] Alexander Greer,[‡,§] Susan D. Richardson,[†] and Linda S. Shimizu*[,†]

[†]Department of Chemistry and Biochemistry, University of South Carolina, Columbia, South Carolina 29208, United States

[‡]Department of Chemistry, Brooklyn College, Brooklyn, New York 11210, United States

[§]Ph.D. Program in Chemistry, Graduate Center of City University of New York, New York, New York 10016, United States

Supporting Information

**ABSTRACT:** Herein, we examine the photochemical formation of reactive oxygen species (ROS) by a porous benzophenone-containing bis-urea host (**1**) to investigate the mechanism of photooxidations that occur within the confines of its nanochannels. UV irradiation of the self-assembled host in the presence of molecular oxygen generates both singlet oxygen and superoxide when suspended in solution. The efficiency of ROS generation by the host is lower than that of benzophenone (BP), which could be beneficial for reactions carried out catalytically, as ROS species react quickly and often unselectively. Superoxide formation was detected through reaction with 5,5-dimethyl-1-pyrroline *N*-oxide in the presence of methanol. However, it is not detected in $CHCl_3$, as it reacts rapidly with the solvent to generate methaneperoxy and chloride anions, similar to BP. The lifetime of airborne singlet oxygen ($\tau_{\Delta airborne}$) was examined at the air−solid outer surface of the host and host·quencher complexes and suggests that quenching is a surface phenomenon. The efficiency of the host and BP as catalysts was compared for the photooxidation of 1-methyl-1-cyclohexene in solution. Both the host and BP mediate the photooxidation in $CHCl_3$, benzene, and benzene-$d_6$, producing primarily epoxide-derived products with low selectivity likely by both type I and type II photooxidation processes. Interestingly, in $CHCl_3$, two chlorohydrins were also formed, reflecting the formation of chloride in this solvent. In contrast, UV irradiation of the host·guest crystals in an oxygen atmosphere produced no epoxide and appeared to favor mainly the type II processes. Photolysis afforded high conversion to only three products: an enone, a tertiary allylic alcohol, and a diol, which demonstrates the accessibility of the encapsulated reactants to oxygen and the influence of confinement on the reaction pathway.

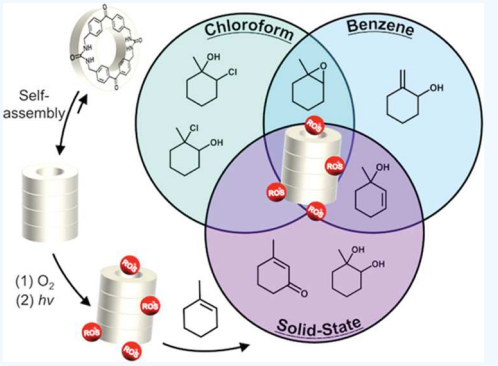


## INTRODUCTION

Here, we investigate the selectivity and efficiency of reactive oxygen species (ROS) photogeneration by a self-assembled benzophenone *bis*-urea macrocycle (host **1**) and probe its utility for mediating the photooxidation of 1-methyl-1-cyclohexene (**2**) suspended in solution compared to the solid state. Host **1** presents two benzophenone (BP) photosensitizer units covalently attached to two urea groups through methylene bridges resulting in a *bis*-urea macrocycle. Self-assembly through bifurcated urea hydrogen-bonding interactions affords hexagonally packed columnar nanotubes that are activated by heating to generate accessible channels that can be readily loaded with guests and applied as a nanoreactor for selective photooxidations, Figure 1.[1,2]

Our previous report showed that photolysis of host **1** crystals in oxygenated $CHCl_3$ showed NIR photoluminescence of $^1O_2$ at 1270 nm.[1] Furthermore, UV irradiation (1 h) of the crystals generates low quantities (~1 in 30 000 molecules) of persistent triplet radical pairs consisting of a ketyl radical and benzylic radicals.[3] In the current work, we hypothesize that host **1** will photogenerate ROS in a controlled manner based on media (suspended in solution versus in the solid state). Our work is fundamental, in that controlling the type of ROS formed is challenging.

ROS can be employed in a diverse range of applications ranging from wastewater treatment to photodynamic therapy for cancer treatment[4−7] but are often produced as mixtures. This is because $O_2$ can be activated through type I and type II photosensitized oxidation processes.[8,9] Type I reactions produce species such as $O_2^{\bullet-}$, $HO_2$·, ROO·, RO·, and ·OH.[9−11] Type II reactions mainly produce singlet oxygen ($^1O_2$) through a Dexter energy transfer of the triplet sensitizer with $^3O_2$.[8,12−14] Achieving high selectivity in photooxidations carried out by ROS is challenging due to their high reactivity. Thus, strategies to achieve control over selectivity are useful

Received: March 26, 2019
Accepted: April 25, 2019
Published: May 8, 2019






DOI: 10.1021/acsomega.9b00831
ACS Omega 2019, 4, 8290−8298

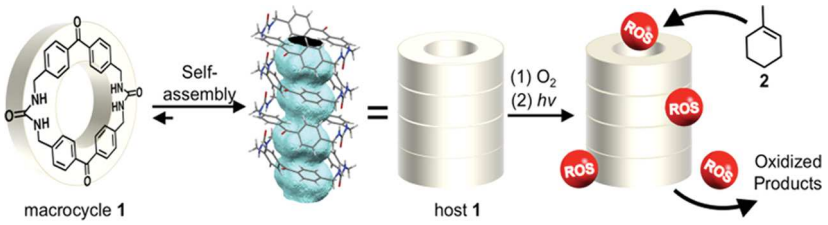


**Figure 1.** Macrocycle **1** is composed of two BP sensitizer units covalently bound through methylene urea groups. Self-assembly through bifurcated urea hydrogen-bonding interactions results in the formation of porous host **1** nanotubes with one-dimensional (1D) elliptical channels (highlighted in light blue). UV irradiation of the host crystals results in the generation of ROS through type I and type II pathways.

**Scheme 1. Proposed Mechanism for the Photooxidation Pathways of Host 1**

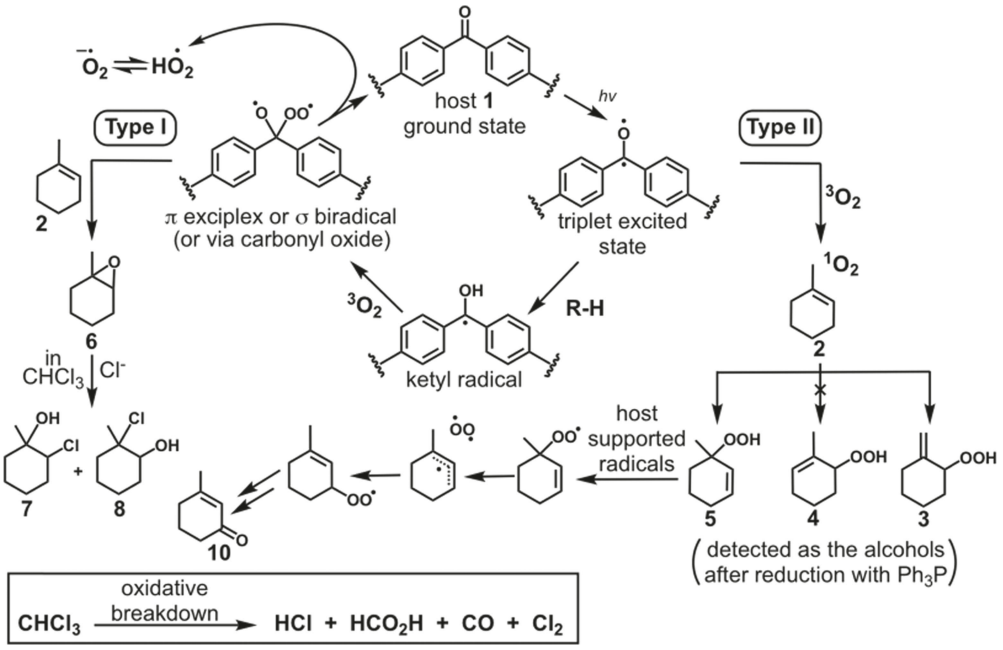


and include templating,[15] air−water interfacial effects,[16] and nanocavity confinement.[1,17,18]

Herein, we probe the channel confinement effect with host **1** in an effort to gain some control over the ROS mechanism. In this work, we found that photolysis of host **1** leads to (1) the detection of both $O_2^{\bullet-}$ and $^1O_2$, which was found to be dependent on its environment; (2) an $^1O_2$ quantum yield ($\Phi[^1O_2]$) of 1−12%; (3) outer wall quenching of $^1O_2$ by host **1**, reducing the lifetime of $^1O_2$ at the air−solid interface; and (4) some selectivity in photooxidations of 1-methyl-1-cyclohexene **2** in solution (type I and type II reactions) versus within the solid phase (favoring type II reactions). Selectivity comparisons of host **1** are made with homogeneous photooxidations with benzophenone[19] and selectivity achieved with octa acid hosts[20] and zeolites.[21]

Our data are consistent with the mechanism shown in Scheme 1, in which host **1** photogenerates both $^1O_2$ and $O_2^{\bullet-}$.[10,22] Selectivity for hydroperoxide **5** over **3** and **4** is seen in the solid state, where **5** undergoes a Schenk rearrangement to enone **10**. Superoxide generation by BP involves the formation of a ketyl radical, which will then undergo an electron-transfer process with $^3O_2$ to form $O_2^{\bullet-}$.[10,22,23] A $\pi$ host/$O_2$ exciplex or $\sigma$ $R_2C(O^{\bullet})O_2^{\bullet}$ biradical at a BP site is proposed as the epoxidizing agent due to the unusual formation of chlorohydrins in $CHCl_3$.

## RESULTS AND DISCUSSION

**ROS Generated by the Host 1 Crystals Suspended in Solution.** The type of ROS generated by host **1** suspended in solution was investigated using electron paramagnetic resonance (EPR) and UV−vis spectroscopies. Literature examples show that BP photoactivates oxygen to $O_2^{\bullet-}$ in protic solvents, such as MeOH, ethanol, and 2-propanol.[10,22] Therefore, EPR spin-trapping experiments were used to probe if host **1**, like parent BP, generates $O_2^{\bullet-}$. 5,5-Dimethyl-1-pyrroline *N*-oxide (DMPO) was selected as the spin trap, which is known to form adducts (doublet of triplets) with $O_2^{\bullet-}$, hydroxide, or peroxyl radicals, where DMPO−OOH degrades to DMPO−OH adduct.[24−26] Interestingly, the detection of $O_2^{\bullet-}$ by EPR was found to be solvent-dependent using DMPO, where the DMPO−OOH adduct was detected in a solution of benzene containing catalytic amounts MeOH but was not detected in $CHCl_3$ (Figure 2).

Irradiation of a host **1** suspension of DMPO in benzene with a catalytic amount of MeOH resulted in the formation of a DMPO adduct evident (Figure 2A) by hyperfine splitting constants of $a^N$ = 14.2 G and $a^H$ = 9.2 G, which is in the range of typical DMPO−OOH adducts (Figure S8).[27−29] Furthermore, the irradiation of BP for 2 min in the presence of DMPO and MeOH also resulted in the formation of a four-line spectrum that overlays well with the spectra obtained by host **1**, with $a^N$ = 13.8 G and $a^H$ = 9.3 G (Figure S9). In the



DOI: 10.1021/acsomega.9b00831
ACS Omega 2019, 4, 8290−8298

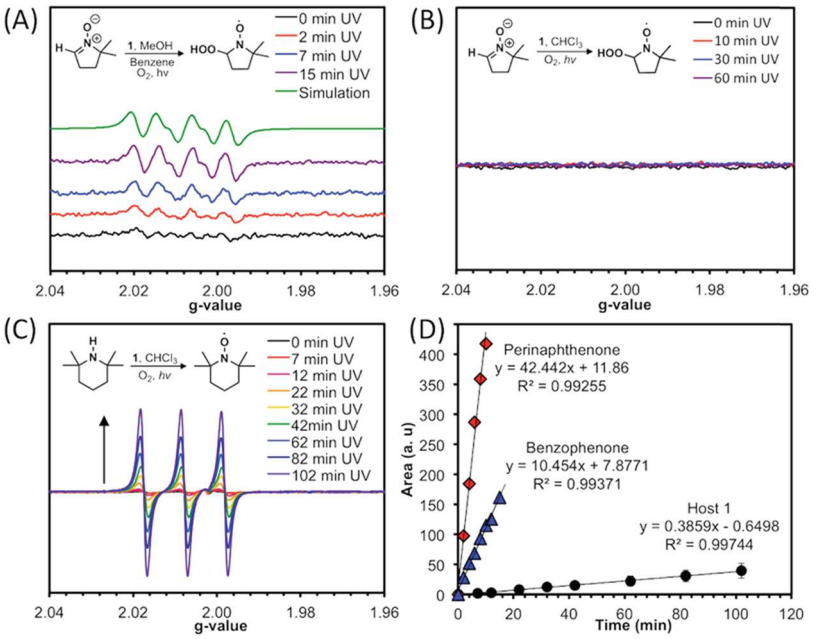


**Figure 2.** EPR studies of host **1** suspended in oxygen-saturated solutions of $O_2^{\bullet-}$ and $^1O_2$ quenchers. (A) DMPO was used to trap $O_2^{\bullet-}$ in benzene in the presence of **1** and MeOH. (B) DMPO $O_2^{\bullet-}$-trapping experiment in $CHCl_3$ in the presence of **1**. (C) Irradiation of **1** in a solution of 2,2,6,6-tetramethylpiperidine (TMP) in $CHCl_3$ results in the chemical quenching of $^1O_2$ to form 2,2,6,6-tetramethyl piperidine-1-yl oxidanyl (TEMPO) over time. (D) Comparison of the TMP chemical-quenching studies with three photosensitizers: perinaphthenone, BP, and host **1**. The error bars for the host **1** plot represent the standard deviation between triplicate trials.

presence of MeOH, the host can generate $O_2^{\bullet-}$, albeit ~15× slower than BP. The formation of superoxide is further supported by the direct detection of its $\lambda_{max}$ at 255 nm, using UV−visible spectroscopy in acetonitrile (Figure S25).[10]

A similar experiment was carried out using chloroform as the solvent; however, no DMPO adduct was detected, Figure 4B. The lack of DMPO adduct suggests that the $[O_2^{\bullet-}]$ is very low, leaving little if any $O_2^{\bullet-}$ to form an adduct with DMPO. Relatedly, Roberts and Sawyer reported that $O_2^{\bullet-}$ reacts with $CHCl_3$ to generate methaneperoxy ($HC(=O)OO^-$) and chloride anions.[30] In addition, the oxidative breakdown of $CHCl_3$ is also known to produce HCl, $HCO_2H$, CO, and $Cl_2$. Therefore, it is likely that $O_2^{\bullet-}$ is indeed generated by **1** in $CHCl_3$ but quickly reacts with the solvent before any DMPO adduct can be formed. This result suggests that the use of $CHCl_3$ for $O_2^{\bullet-}$ detection by DMPO should be avoided.

Next, the formation of $^1O_2$ was probed using 2,2,6,6-tetramethylpiperidine (TMP), which is oxidized by $^1O_2$ to form a stable nitroxide radical 2,2,6,6-tetramethyl piperidine-1-yl oxidanyl (TEMPO), which gives rise to three-line EPR spectra.[24,26] Irradiation of an oxygen-saturated $CHCl_3$ solution with suspended host **1** led to the formation of a three-line TEMPO signal, indicating the formation of $^1O_2$ (Figure 2C). The areas obtained by the EPR signals for DMPO and TEMPO in $CHCl_3$ were found to be quite similar (5.8 vs 5.1) with the $O_2^{\bullet-}$ adduct generated ~1.1× faster than $^1O_2$. Thus, both $O_2^{\bullet-}$ and $^1O_2$ are photogenerated by host **1** in type I and type II processes.

**Quantum Yields of $^1O_2$ Generation in Solution.** The $^1O_2$ quantum yield of **1** while suspended in $CHCl_3$ was approximated using EPR and UV−visible spectroscopy and was found to be low, ranging from 1 to 12% depending on the method. Figure 2C shows the gradual formation of TEMPO from TMP. The $\Phi[^1O_2]^{host\ 1}$ was estimated to be ~1% in $CHCl_3$ when compared to the reference, perinapthenone (Figure 2D).[31] In some cases, the use of TMP in determining the quantum yield of $^1O_2$ production can be misleading when the excited photosensitizer is able to react with TMP, resulting in the $TMP^{+\bullet}$.[26] The radical cation can then undergo a reaction with molecular oxygen to form an EPR-detectable TEMPO signal that is not attributed to $^1O_2$ production.[26] While this process has been observed by the parent BP, it is not anticipated to occur (or be minimal at best) with host **1** because TMP is too large to fit into the host channels (Table S1).

In addition to EPR, the $\Phi[^1O_2]$ was also measured by UV−vis spectroscopy using 1,4-dimethylnaphthalene (DMN), an $^1O_2$ trap that absorbs at higher-energy wavelengths (~290 nm) than the 360 nm required for **1** to generate $^1O_2$. Figure 3 shows the decrease of the DMN absorbance signal with the time of irradiation, indicative of the DMN reaction with $^1O_2$ forming the 1,4-naphthalene endoperoxide product, which does not absorb in this region. From these data, we calculated the $\Phi[^1O_2]^{host\ 1}$ to be 12% in $CHCl_3$, when compared to the

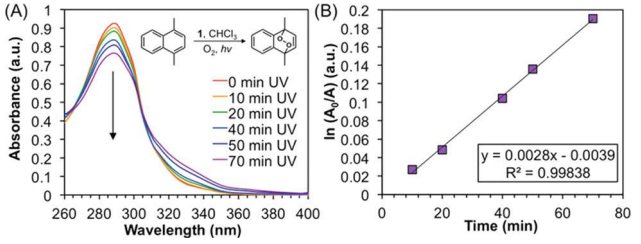


**Figure 3.** Indirect quantification of the quantum yield of $^1O_2$ generation by host **1** as monitored by the absorption loss of DMN. (A) Oxygen-saturated solution of DMN was irradiated in the presence of host **1** and the absorbance spectra recorded over time to monitor the loss of DMN. (B) Area of UV absorbance plotted versus time of UV irradiation for host **1**.



DOI: 10.1021/acsomega.9b00831
ACS Omega 2019, 4, 8290−8298

reference methylene blue.[32,33] We note that 1,4-dimethylnaphthalene-1,4-endoperoxide has a half-life ($t_{1/2}$) of 5 h at 25 °C and can serve as a chemical source of $^1O_2$;[34−36] however, this $^1O_2$ release was relatively low on the time scale of our quantum yield measurements. Furthermore, it is not surprising that the $\Phi[^1O_2]$ varies between the two techniques, as they show different sensitivity.[37]

Given these results, we conclude that the host generates low quantities of $^1O_2$ with $\Phi[^1O_2]^{host\ 1}$ ranging from 1 to 12%. The low $^1O_2$ quantum yield could be advantageous for suspended host catalytic studies, as it may encourage oxidations to occur within the confines of the host channels as opposed to free in solution.

**Lifetime of $^1O_2$ at the Air−Solid Interface.** Because selectivity was reported for the photooxidation of 2-methyl-2-butene in crystalline complexes with host **1**,[1] we are interested in the lifetime of $^1O_2$ at the air−solid interface of the host crystals. The lifetime reduction of $^1O_2$ by the **1**·DMSO complex and by solid $Ph_3P$ was measured to give a sense of the outer-wall-quenching capacity. Solid $Ph_3P$ was used for comparison, as it is a well-known chemical quencher of $^1O_2$ in the solution phase.[13,38] Other **1**·quencher complexes were prepared and include *N*,*N*-dimethylaniline, pyridine, and *N*,*N*,*N*′,*N*′-tetramethyl-ethane-1,2-diamine (Table S1).

Figure 4 shows the lifetime of airborne $^1O_2$ ($\tau_{\Delta airborne}$) generated by a three-phase apparatus to be ∼150 μs and thus

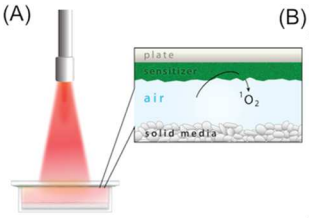


(B)

| Entry | Sample | $\tau_{\Delta airborne}$(ms) |
|---|---|---|
| 1 | Pc plate | ~0.15 |
| 2 | **1**•DMSO + Pc plate | 0.13±0.02 |
| 3 | **1**•pyridine +Pc plate | 0.12±0.06 |
| 4 | Solid $Ph_3P$ +Pc plate | 0.10±0.03 |

**Figure 4.** Measurement of the airborne $^1O_2$ lifetime at the air−solid interface. (A) Simplified experimental setup, consisting of a sensitizer plate used to generate airborne $^1O_2$ whose lifetime was measured by a photomultiplier tube through a 1270 nm band-pass filter. (B) Table of the experimental $^1O_2$ lifetimes obtained in this study.

longer compared to $^1O_2$ solvated in benzene and toluene by ∼5-fold (31 and 29 μs, respectively), and MeOH and ethanol by ∼15-fold (10 and 13 μs, respectively).[39] The lifetime of $^1O_2$ in DMSO is 30 μs but is reduced in pyridine (5.7 μs).[39] The total quenching rate constant ($k_T$) for $Ph_3P$ is $8.5 \times 10^6$ $M^{-1}$ $s^{-1}$, and for other phosphines, it ranges from 0.1 to $2.0 \times 10^7$ $M^{-1}$ $s^{-1}$.[38,40,41] The table in Figure 4 shows that the $\tau_{\Delta airborne}$ is reduced going from a sample absent of a solid-trapping agent (∼0.15 ms) to a sample containing solid host **1** (with DMSO or pyridine guests; 0.13 and 0.12 ms, respectively) and solid $Ph_3P$ (0.10 ms). These data are in line with the quenching of $^1O_2$ in the solution phase. We attribute the decrease to be sensitive to factors such as the high oxophilicity of $Ph_3P$ in solid-surface physical and chemical quenching. That is, once the $^1O_2$ was carried from the sensitizer plate to the air/solid interface of the solid host or solid $Ph_3P$, it was quenched. In the previous work, long and short $^1O_2$ lifetimes were found depending on whether it resided within a gas bubble or in the bulk aqueous solution.[42] In a gas bubble, an $^1O_2$ lifetime of 0.98 ms has been previously observed.[42] Seeing that the lifetime of $^1O_2$ in air is decreased in the presence of the host in comparison to the Pc plate or in a gas bubble, we wanted to next investigate ROS formation by the interior of the host.

**Comparison of Photooxidations of 1-Methyl-1-cyclohexene (2) Sensitized by Host 1 and BP.** Oxidation reactions were investigated in solution ($CHCl_3$, benzene, and benzene-$d_6$) and in the solid state to uncover differences in product distributions. Our goal is to correlate the products formed to specific photooxidation mechanisms (type I vs type II) and to uncover confinement effects. Substrate **2** and sensitizer (**1** or BP) were UV-irradiated in an oxygen-saturated environment (solution or solid state). The reactions were quenched with triphenylphosphine to reduce any hydroperoxides and analyzed by gas chromatography mass spectrometry (GC−MS) (Table 1).

**Efficiency of Photooxidations in Heterogeneous Solutions.** The photosensitizers investigated vary in solubility. Host **1** was used as a suspension, while BP was soluble. Photolysis of **2** mediated by sensitizer **1** in oxygen-saturated $CHCl_3$ (Table 1, entry 1) led to three major oxidation products, epoxide **6** (21%) and two chlorohydrins **7** (24%) and **8** (16%). Overall, 92% conversion was observed with other minor products consisting mainly of enones and ketones (Figure S20). The formation of the chlorohydrins reflects the degradation of the solvent by $O_2^{\bullet-}$, as indicated by the DMPO spin-trapping experiment in $CHCl_3$. Thus, we compared photolysis of **2** with BP sensitizer under similar conditions (Table 1, entry 2), which resulted in 100% conversion of **2**. Chlorohydrin **7** (37%) was the major product with multiple

**Table 1. Product Distributions in Photosensitized Oxidation of Alkenes**[a]

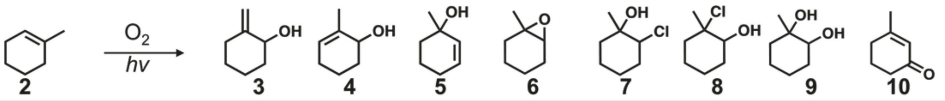


| Entry | Conditions | Time (h) | % Conversion | % Selectivity | | | | | | | |
|---|---|---|---|---|---|---|---|---|---|---|---|
| 1 | Host **1** ($CHCl_3$)[b] | 18 | 92% | -- | -- | -- | 21% | 24% | 16% | -- | -- |
| 2 | BP ($CHCl_3$) | 18 | ∼100% | -- | -- | -- | -- | 37% | -- | -- | -- |
| 3 | Host **1** (benzene)[b] | 12 | 40% | 15% | -- | 29% | 28% | -- | -- | -- | -- |
| 4 | BP (benzene) | 12 | 41% | 6% | -- | 44% | 21% | -- | -- | -- | -- |
| 5 | Host **1** (benzene-$\delta_6$)[b] | 12 | 37% | 11% | -- | 18% | 25% | -- | -- | -- | -- |
| 6 | BP (benzene-$\delta_6$) | 12 | 73% | 29% | -- | 32% | 9% | -- | -- | -- | -- |
| 7 | Host **1** (solid-state) | 5 | 97% | -- | -- | 32% | -- | -- | -- | 13% | 42% |

[a]Product distribution of the most prominent products formed by photooxidation. [b]Indicates that the photosensitizer was suspended in the solvent.



DOI: 10.1021/acsomega.9b00831
ACS Omega 2019, 4, 8290−8298

chlorinated alkenes, again confirming the degradation of $CHCl_3$ under these conditions.

With both sensitizers, epoxide-derived products are observed as well as chloride addition from the oxidative breakdown of solvent (Scheme 1, inset). Our hypothesis is that the epoxidizing agent is either a $\pi$ BP/$O_2$ exciplex or $\sigma$ $R_2C(O^{\bullet})O_2^{\bullet}$ biradical. Benzophenone has been reported to be an n−$\pi^*$ triplet sensitizer, where cycloaddition to an alkene forms a dioxetane in addition to an allylic hydroperoxide formation from singlet oxygen.[19,43] BP is also a noted type I photosensitizer.[44−46] To avoid chloride production, we next examined these reactions in benzene.

Photolysis of **2** mediated by sensitizer **1** for 12 h in oxygen-saturated benzene or benzene-$d_6$ (Table 1, entries 3 and 5) gave similar conversions (40 vs 37%) despite a large variation of the $^1O_2$ lifetime from 30 to 731 $\mu$s.[47] Similarly, poor selectivity was seen in both cases with the major products being alcohols **3**, **5**, and epoxide **6**. In comparison, the photooxidation of **2** sensitized by BP under similar conditions was also unselective and gave the same major products **3**, **5**, and **6** (Table 1, entries 4 and 6). Interestingly, in the case of BP, the 25-fold difference in $^1O_2$ lifetime did play a role in conversion. Nearly, double the conversion of **2** was observed in benzene-$d_6$ (71%) compared to that in benzene (41%). Alcohols **3** and **5** are common oxidation products observed in type II $^1O_2$-mediated oxidations of cycloalkene **2**.[17,48−50] Furthermore, epoxide **6** could arise from either a type I or a type II process. We also observed the formation of significant amounts of biphenyl, which is expected to proceed via H-abstraction and coupling. Lack of mechanistic control likely lowers the selectivity in solution. The biradical is directed to the exterior of the assembled host and is not expected to be influential in reactions that proceed within its interior, for example, within the solid host·guest crystals.

Activated host **1** crystals were readily loaded with alkene **2** to afford a host/guest complex with a 2:1 stoichiometry. Remarkably, the photolysis of host **1**·**2** crystals in the solid state led to only three products in high conversion with shorter irradiation time (Table 1, entry 7). After just 5 h at 0 °C, two unexpected products were obtained, enone **10** (42%) and diol **9** (13%). Products **9** and **10** are not observed in solution, demonstrating the influence encapsulation of **2** on the photooxidation pathway. Indeed, the low temperature ensures that **2** remains in the channel during the photoreaction (Figure S19). Products are not released until the host is sonicated in a tetrahydrofuran (THF) solution of triphenylphosphine. A depiction of a potential host **1**·**2** complex is shown in Figure 5A. The high conversion demonstrates that oxygen readily enters the channels under these conditions. The only typical product observed was alcohol **5**, which was produced in 32% selectivity. Enone **10** is likely derived from $^1O_2$ through a Schenck allylic peroxyl radical rearrangement of **5**.[51,52] This rearrangement may be facilitated by confinement as well as by long-lived resonance-stabilized surface/host radicals, which form in low quantity (up to ∼1 in 10 000 molecules) upon irradiation of host **1** crystals, shown schematically in Figure 5B.[3]

Formation of diol **9** is particularly interesting and may suggest the formation of dioxetane-type intermediates within the narrow channels, Figure 5C. We are currently utilizing computations to investigate the stability of such intermediates within our frameworks. This diol can also be formed upon oxidation of **2** by enzyme P450.[53,54] In contrast to the solution,

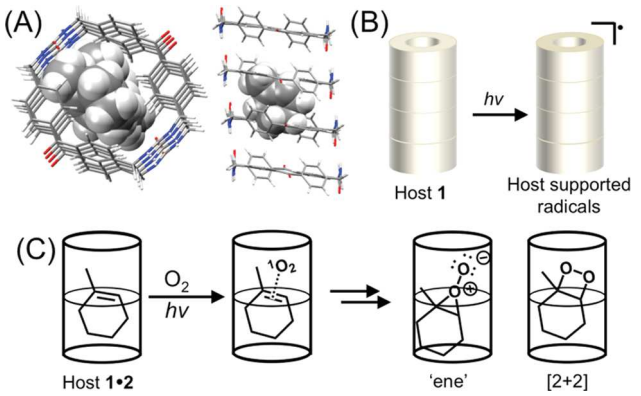


**Figure 5.** Depictions of host **1** complexes. (A) Top-down view (left) and side view (right) of the plausible host **1**·**2** complex. (B) Irradiation of the host **1** nanotubes results in the formation of host-supported radicals in low quantities.[3] (C) Vapor diffusion of **2** resulted in the formation of the host **1**·**2** complex, irradiation in an oxygen atmosphere results in the type II photooxidations via the "ene" or [2 + 2] cycloaddition pathways.

no epoxide was observed within the solid complexes. One plausible explanation is that the required biradical would not be accessible as it is formed on the exterior of host **1**. Thus, it is not surprising that no epoxide was observed.

In comparison to other molecular containers, the reaction of **2** encapsulated in Gibb's octa acid capsule (2:2) with the sensitizer, rose Bengal, in the surrounding $D_2O$ solution favors the tertiary alcohol **5** with 90% selectivity at 60% conversion.[17] Individual octa acid cavitands have a deep cavity (13.73 Å) with a diameter of 11.36 Å to readily uptake guest molecules.[49] Hydrogen-bonding interactions allow two octa acid cavitands to form a closed capsule, which gives a discrete quaternary complex.[49] Interestingly, the hydroperoxide formed was stable in the capsule and showed no rearrangement to **10**. In comparison, host **1** displays a roughly elliptical one-dimensional channel of ∼150 $\mu$M in length with only two entrances and a diameter of 5 × 7.1 Å$^2$ (Figure 1, the channel highlighted in blue). Absorbed guests are trapped within the confined environment under these conditions and the ROS must diffuse within the long channels. Thus, host **1** is more similar to zeolites, such as ZSM-5 zeolite, which has both straight and elliptical pores with dimensions of approximately 5.2 × 5.8 Å$^2$. Photolysis of **2** in ZSM-5 forms alcohols **3**, **4**, and **5** upon photooxidation and subsequent reduction.[50] The selectivity of alkene photooxidation can be improved in cation-exchanged zeolites.[55−57] For example, Na-ZSM-5 Y-type zeolite produced secondary allylic alcohol **3** with 88% selectivity.[50] From the reactant's perspective, photooxidation in the "infinite" 1D channels of host **1** is a significantly different environment than in distinct molecular capsules.

In summary, the photooxidation studies of cyclohexene **2** in solution and in the solid state are consistent with the proposed mechanism in Scheme 1. Our findings shed light on the complex mechanistic pathways of photooxidations and highlight degradation reactions that are detrimental to selectivity. (i) $O_2^{\bullet-}$ and BP/$O_2$ exciplexes are important in solution, leading to the oxidative degradation of $CHCl_3$ and subsequent formation of chlorinated products. These biradical intermediates are likely also responsible for the formation of significant amounts of biphenyl observed in reactions carried out in



DOI: 10.1021/acsomega.9b00831
ACS Omega 2019, 4, 8290−8298

benzene. Epoxide formation that was observed in the solution could arise from either a type I or a type II process.

(ii) $^1O_2$ is important in the solid-state reaction. Cyclohexene **2** is a good match for the size and shape of the host **1** channel and forms 2:1 host/guest complexes. The encapsulated cyclohexene is accessible to oxygen gas and upon irradiation likely undergoes ene reactions with $^1O_2$.[17,49,50,58] Encapsulation dramatically influences the products observed. In particular, high selectivity was observed for **5**, which undergoes efficient allylic peroxyl radical rearrangement to enone **10** within the narrow channels. This pathway appears to represent the majority of the products (**5** + **10** ∼74%). The unexpected diol **9**, observed within our crystalline host, may be due to steric constraints that aid the [2 + 2] process to give a proposed dioxetane intermediate (Figure 5C), which subsequently affords the observed diol either upon rearrangement in the channel or upon extraction into a solution of triphenylphosphine. The high conversion suggests that ROS readily diffuses along the ∼150 $\mu$M channels.

(iii) The lifetime of airborne $^1O_2$ was also examined at the air−solid outer surface of the host. Airborne $^1O_2$ was generated by a Pc plate that was physically isolated from the host in the solid state. Minimal reduction in the lifetime of airborne $^1O_2$ was observed when it came in contact with the surface of host **1**. The data suggest that $^1O_2$ quenching is a surface phenomenon. Thus, we propose that $^1O_2$ via the type II process is involved in the air/solid reaction with cyclohexene **2** and is primarily within the confined channels of host **1**.

## CONCLUSIONS

The assembled host **1** displays markedly different behaviors of ROS generated upon photolysis in solution and in the solid state. UV irradiation of photosensitizers host **1** and BP leads to the production of both $^1O_2$ and $O_2^{\bullet-}$ in solution. These represent key reactive species formed in the type I and type II mechanisms. These species undergo unselective reactions with 1-methyl-1-cyclohexene to afford epoxide-derived products as well as degradation of the solvent, which generated chloride in $CHCl_3$ and biphenyl in benzene. It would be advantageous to be able to select a single ROS to direct more selective photooxidations.

In contrast, within the nanochannels of the host in the solid state, mainly type II ($^1O_2$) processes were observed. UV irradiation of the crystalline host·guest complex in an oxygen atmosphere produced no epoxide and afforded the tertiary alcohol **5** with enone **10** as a downstream product of **5**. An unexpected diol, **9**, is proposed to form via formally a [2 + 2]-mediated dioxetane in confinement. Overall, while both $^1O_2$ and $O_2^{\bullet-}$ have access to the channels of **1**, it appears that $^1O_2$ is the main reactive species with the bound cyclohexene **2**. Comparison of reactions carried out in the air/solid and solution/solid interfaces suggests that selectivity arises primarily in the interior of the host. This is likely a result of confinement and/or directed mobility of ROS within the elliptical subnanometer channels. We are currently investigating the use of molecular dynamics to probe complexes of host **1** with $O_2^{\bullet-}$ and $^1O_2$ to see if these ROS species diffuse freely or adhere to the walls. In particular, how does the encapsulation of ROS species within nanochannels affect the mobility, lifetime, and stability of the proposed intermediates? A greater understanding of conditions that favor control over the selectivity of ROS generation and their mobility within confined environments would help in the development of more selective, next-generation photooxidation catalysts.

## EXPERIMENTAL SECTION

**Materials and Reagents.** BP, benzophenone; $CHCl_3$, chloroform; MeOH, methanol; DMPO, 5,5-dimethyl-1-pyrroline *N*-oxide; $Ph_3P$, triphenylphosphine; DMSO, dimethylsulfoxide; TMP, 2,2,6,6-tetramethylpiperidine; TEMPO, 2,2,6,6-tetramethyl piperidin-1-yl oxidanyl; AlPcS, Al(III) phthalocyanine tetrasulfonate; Pc, phthalocyanine.

**Host Synthesis and Guest Encapsulation.** Host **1** was synthesized as previously reported.[1−3] Crystallization by slow cooling in DMSO (10 mg/mL) affords white needle-like crystals with regular channels (7.1 × 5.0 Å$^2$) that are filled with DMSO.[1−3] The host crystals were activated by heating to 180 °C using thermogravimetric analysis (TGA) at a ramp rate of 4 °C/min.[1−3] Once activated, the evacuated host can be readily loaded with guest molecules by soaking the crystals in guest solutions or through vapor diffusion.[1,2]

**Photolysis.** Irradiations were carried out in a Rayonet reactor at 350 nm in Norell quartz EPR tubes or sodium borosilicate vials.

**EPR Spectroscopy.** EPR was used to probe the types of ROS generated by host **1** upon UV irradiation while suspended in solution. In each experiment, the sensitizer (**1** or a standard) was added to oxygen-saturated stock solutions containing known ROS quenchers such as TMP, DMPO, or DMN. The solutions were UV-irradiated at 360 nm in a Rayonet reactor, and the reaction was monitored over time by EPR or UV−visible spectroscopy. More detail for each experiment can be found in the Supporting Information.

**Quantum Yield Measurement by EPR.** The $^1O_2$ quantum yield ($\Phi[^1O_2]$) was determined by plotting the area of TEMPO EPR signal versus time and obtaining the slope of each plot using the equation $\Phi[^1O_2]^{sample} = \Phi[^1O_2]^{ref}(m^{sample}/m^{ref})$, where perinaphthenone was used as the reference ($\Phi[^1O_2]^{ref}$ = 0.97 in $CHCl_3$), $m^{sample}$ is the slope of the host plot, and $m^{ref}$ is the slope of the perinaphthenone plot (Figure 2D).[26,31] By this method, we estimate the $\Phi[^1O_2]^{host\ 1}$ to be ∼1% in $CHCl_3$.

**Quantum Yield Measurement by UV−Visible Spectroscopy.** The $^1O_2$ quantum yield ($\Phi[^1O_2]$) was determined by plotting the difference between each absorbance signal versus time and obtaining the slope of each plot using the equation $\Phi[^1O_2]^{sample} = \Phi[^1O_2]^{ref}(m^{sample}/m^{ref})$, where methylene blue was used as the reference ($\Phi[^1O_2]^{ref}$ = 0.52 in $CHCl_3$), $m^{sample}$ is the slope of the host plot, and $m^{ref}$ is the slope of the methylene blue plot.

**Lifetime of $^1O_2$ at the Air−Solid Interface.** An apparatus was constructed to deliver airborne $^1O_2$ to a solid-quenching agent. The reactor consisted of a sensitizing glass plate made by depositing Al(III) phthalocyanine tetrasulfonate (AlPcS) (∼5 × 10$^{-5}$ mol) onto the bottom side of a porous silica square (0.50 g, shape: 1.0 mm × 2.25 cm$^2$). A 0.8 mM solution of AlPcS in MeOH was deposited on the bottom face of the plate via slow evaporation. The glass plate was placed sensitizer-face down on top of a custom-made plate containing a well (sized: 1 mm × 1 cm × 1 cm). The solid trapping agent (10 mg) was placed in the well. The sensitizer plate was not in contact with the solid trapping agent and sat above it by 0.1 mm. A digital ruler with a precision of 0.01 mm was used to measure the distance between the sensitizer plate and the solid trapping agent in the well. The sensitizer plate was placed 3.0



DOI: 10.1021/acsomega.9b00831
ACS Omega 2019, 4, 8290−8298

cm below a terminus of a multimode FT-400-EMT optical fiber with an SMA 905 connector (Thorlabs, Inc.). The optical fiber was connected to a 630 nm light source from a Nd:YAG Q-switched laser pumping an optical parametric oscillator producing 5 ns ∼0.2 mJ/pulses. The output of the 630 nm light from the laser yielded incident photons in a Gaussian distribution upon the sensitizer plate. The $^1O_2$ luminescence was detected by a photomultiplier tube (H10330A-45, Hamamatsu Corp.) through a 1270 nm band-pass filter (FWHM = 15 nm). The $^1O_2$ luminescence signals were registered on a 600 MHz oscilloscope, and the kinetic data for the $^1O_2$ lifetime ($\tau_{\Delta airborne}$) were determined by a least-square curve-fitting procedure. The $^1O_2$ decay was observed in the 1270 nm phosphorescence upon irradiation of the sensitizer particles with 630 nm light. A slow component for the $^1O_2$ signal was observed (tenths of microseconds), which is attributed to airborne $^1O_2$ in the air gap between the sensitizer plate of origin and the solid trapping agents. A reduction of the $^1O_2$ lifetime ($\tau_{\Delta airborne}$) arises when the $^1O_2$ encounters the air/solid interface of the trapping agent.

**Host 1 in Photooxidations.** Photooxidations by host **1** in $CHCl_3$ and benzene resulted in multiple products, and characterization was attempted only on key products. Relative conversion and selectivity were obtained by gas chromatography mass spectrometry (GC−MS), and the products were confirmed using standards and/or the NIST database and literature when applicable (Supporting Information Figures S20−S23).

**Host 1 in Photooxidations in Solution.** Cycloalkene **2** (21 mM) was stirred in oxygenated $CHCl_3$ or benzene with host **1** (2 mg, 20 mol %). The photooxidations in $CHCl_3$ were UV-irradiated for 18 h and diluted with $CH_2Cl_2$ solutions of triphenylphosphine (21 mM) for rapid analysis by GC−MS. The photooxidations in benzene were UV-irradiated over time, and aliquots (50 μL) of the reaction mixture were removed over time (4, 8, and 12 h), diluted into solutions of triphenylphosphine in benzene.

**Host 1 Loading with Cycloalkene 2.** The activated host was equilibrated with **2** for at least 24 h. TGA of the host **1**·**2** complex displayed one-step desorption from 25 to 80 °C with a weight loss of 8.2% (Figure S19 and Table S1). The host·guest stoichiometry was calculated from the weight loss and corresponded to a 2:1 host/guest ratio. Because the TGA indicates that alkene **2** slowly desorbs from the host at ambient temperature, all solid-state reactions were performed at lower temperatures (0 °C).

**Solid-State Host 1 in Photooxidations.** Host **1** (∼16 mg) was UV-irradiated in a borosilicate vial saturated with oxygen for 5 h at 0 °C. After irradiation, the complex was immediately sonicated in a solution of triphenylphosphine (21 mM in THF) and analyzed by GC−MS.

## ■ ASSOCIATED CONTENT

### Supporting Information

The Supporting Information is available free of charge on the ACS Publications website at DOI: 10.1021/acsomega.9b00831.

$^1$H NMR of 4,4′-bis(bromomethyl)benzophenone (Figure S1); $^1$H NMR of protected benzophenone *bis*-urea macrocycle **1** (Figures S2); $^1$H NMR of benzophenone *bis*-urea macrocycle **1** (Figures S3); space-filling model of **1** (Figure S4); self-assembly of macrocycle **1** (Figure S5); decolorization of DMPO in MeOH (Figure S6); EPR spectra (Figures S7−S14); EPR spectral simulation (Figures S8 and S9); comparison of area obtained in the formation of TEMPO (Figure S15); singlet oxygen quantum yield (Figure S16); absorption data (Figure S17); comparison of absorptions (Figure S18); TGA plots (Figure S19); GC−MS data (Figure S20); GC trace (Figures S21−S23); airborne singlet oxygen decay curve (Figure S24); direct detection of superoxide (Figure S25); and EPR spin-trapping study (Figure S26) (PDF)

## ■ AUTHOR INFORMATION


### Corresponding Author

*E-mail: shimizls@mailbox.sc.edu.

### ORCID

Hannah K. Liberatore: 0000-0001-7423-3251
Alexander Greer: 0000-0003-4444-9099
Susan D. Richardson: 0000-0001-6207-4513
Linda S. Shimizu: 0000-0001-5599-4960


### Author Contributions

The manuscript was written through contributions of all authors.

### Notes

The authors declare no competing financial interest.

## ■ ACKNOWLEDGMENTS

B.A.D. and L.S.S. acknowledge support from the National Science Foundation (CHE-1608874 and OIA-1655740) and a SPARC Graduate Research Grant from the Office of the Vice President for Research at the University of South Carolina. A.G. acknowledges support from the National Science Foundation (CHE-1464975).

## ■ REFERENCES


(1) Geer, M. F.; Walla, M. D.; Solntsev, K. M.; Strassert, C.; Shimizu, L. S. Self-assembled benzophenone bis-urea macrocycles facilitate selective oxidations by singlet oxygen. *J. Org. Chem.* **2013**, *78*, 5568−5578.

(2) Dewal, M. B.; Xu, Y.; Yang, J.; Mohammed, F.; Smith, M. D.; Shimizu, L. S. Manipulating the cavity of a porous material changes the photoreactivity of included guests. *Chem. Commun.* **2008**, 3909−3911.

(3) DeHaven, B. A.; Tokarski, J. T.; Korous, A. A.; Mentink-Vigier, F.; Makris, T. M.; Brugh, A. M.; Forbes, M. D. E.; van Tol, J.; Bowers, C. R.; Shimizu, L. S. Persistent radicals of self-assembled benzophenone bis-urea macrocycles: Characterization and application as a polarizing agent for solid-state DNP MAS Spectroscopy. *Chem. - Eur. J.* **2017**, *23*, 8315−8319.

(4) DeRosa, M.; Crutchley, R. Photosensitized singlet oxygen and its applications. *Coord. Chem. Rev.* **2002**, *233*−*234*, 351−371.

(5) Kim, H.; Kim, W.; Mackeyev, Y.; Lee, G.-S.; Kim, H.-J.; Tachikawa, T.; Hong, S.; Lee, S.; Kim, J.; Wilson, L. J.; Majima, T.; Alvarez, P. J. J.; Choi, W.; Lee, J. Selective oxidative degradation of organic pollutants by singlet oxygen-mediated photosensitization: Tin porphyrin versus $C_{60}$ aminofullerene systems. *Environ. Sci. Technol.* **2012**, *46*, 9606−9613.

(6) Ogilby, P. R. Singlet oxygen: there is indeed something new under the sun. *Chem. Soc. Rev.* **2010**, *39*, 3181−3209.

(7) Dąbrowski, J. M. Reactive oxygen species in photodynamic therapy: Mechanisms of their generation and potentiation. *Adv. Inorg. Chem.* **2017**, *70*, 343−394.

(8) Ghogare, A. A.; Greer, A. Using singlet oxygen to synthesize natural products and drugs. *Chem. Rev.* **2016**, *116*, 9994−10034.




DOI: 10.1021/acsomega.9b00831
*ACS Omega* 2019, 4, 8290−8298

(9) Baptista, M. S.; Cadet, J.; Di Mascio, P.; Ghogare, A. A.; Greer, A.; Hamblin, M. R.; Lorente, C.; Nunez, S. C.; Ribeiro, M. S.; Thomas, A. H.; Vignoni, M.; Yoshimura, T. M. Type I and Type II photosensitized oxidation reactions: Guidelines and mechanistic pathways. *Photochem. Photobiol.* **2017**, *93*, 912−919.
(10) Hayyan, M.; Hashim, M. A.; AlNashef, I. M. Superoxide ion: Generation and chemical implications. *Chem. Rev.* **2016**, *116*, 3029−3085.
(11) Lee-Ruff, E. The organic chemistry of superoxide. *Chem. Soc. Rev.* **1977**, *6*, 195−214.
(12) Skourtis, S. S.; Liu, C.; Antoniou, P.; Virshup, A. M.; Beratan, D. N. Dexter energy transfer pathways. *Proc. Natl. Acad. Sci. U.S.A.* **2016**, *113*, 8115−8120.
(13) Greer, A. Christopher Foote's discover of the role of singlet oxygen [$^1O_2(^1\Delta_g)$] in photosensitized oxidation reactions. *Acc. Chem. Res.* **2006**, *39*, 797−804.
(14) Foote, C. S.; Wexler, S. Olefin oxidations with excited singlet molecular oxygen. *J. Am. Chem. Soc.* **1964**, *86*, 3879−3880.
(15) Wiegand, C.; Herdtweck, E.; Bach, T. Enantioselectivity in visible light-induced, singlet oxygen [2+4] cylcoaddition reactions (type II photooxygenations) of 2-pyridones. *Chem. Commun.* **2012**, *48*, 10195−10197.
(16) Malek, B.; Fang, W.; Abramova, I.; Walalawela, N.; Ghogare, A. A.; Greer, A. "Ene" reactions of singlet oxygen at the air-water interface. *J. Org. Chem.* **2016**, *81*, 6395−6401.
(17) Natarajan, A.; Kaanumalle, L. S.; Jockusch, S.; Gibb, C. L. D.; Gibb, B. C.; Turro, N. J.; Ramamurthy, V. Controlling photoreactions with restricted spaces and weak intermolecular forces: Exquisite selectivity during oxidation of olefins by singlet oxygen. *J. Am. Chem. Soc.* **2007**, *129*, 4132−4133.
(18) Chen, Y.-Z.; Wang, Z. U.; Wang, H.; Lu, J.; Yu, S.-H.; Jiang, H.-L. Singlet oxygen-engaged selective photo-oxidation over Pt nanocrystals/porphyrinic MOF: The role of photothermal effect and Pt electronic state. *J. Am. Chem. Soc.* **2017**, *139*, 2035−2044.
(19) Shimizu, N.; Bartlett, P. D. Photooxidation of olefins sensitized by α-diketones and by benzophenone. A practical epoxidation method with biacetyl. *J. Am. Chem. Soc.* **1976**, *98*, 4193−4200.
(20) Gupta, S.; Ramamurthy, V. Characterization and singlet oxygen oxidation of 1-alkyl cyclohexenes encapsulated within a water-soluble organic capsule. *ChemPhotoChem* **2018**, *2*, 655−666.
(21) Pace, A.; Clennan, E. L. A new experimental protocol of intrazeolite photooxidations. The first product-based estimate of an upper limit for the intrazeolite singlet oxygen lifetime. *J. Am. Chem. Soc.* **2002**, *124*, 11236−11237.
(22) McDowell, M. S.; Bakac, A.; Espenson, J. H. A convenient route to superoxide ion in aqueous solution. *Inorg. Chem.* **1983**, *22*, 847−848.
(23) Sun, G.; Hong, K. H. Photo-induced antimicrobial and decontaminating agents: Recent progresses in polymer and textile applications. *Text. Res. J.* **2013**, *83*, 532−542.
(24) Nosaka, Y.; Nosaka, A. Y. Generation and detection of reactive oxygen species in photocatalysis. *Chem. Rev.* **2017**, *117*, 11302−11336.
(25) He, W.; Liu, Y.; Wamer, W. G.; Yin, J.-J. Electron spin resonance spectroscopy for the study of nanomaterial-mediated generation of reactive oxygen species. *J. Food Drug Anal.* **2014**, *22*, 49−63.
(26) Nardi, G.; Manet, I.; Monti, S.; Miranda, M. A.; Lhiaubet-Vallet, V. Scope and limitations of the TEMPO/EPR method for singlet oxygen detection: the misleading role of electron transfer. *Free Radical Biol. Med.* **2014**, *77*, 64−70.
(27) Buettner, G. R. Spin trapping: ESR parameters of spin adducts. *Free Radical Biol. Med.* **1987**, *3*, 259−303.
(28) Zang, L.-Y.; Misra, H. P. EPR kinetic studies of superoxide radicals generated during the autooxidation of 1-methyl-4-phenyl-2,3-dihydropyridinium, a bioactivated intermediate of parkinsonian-inducing neurotoxin 1-methyl-4-phenyl-1,2,3,6-tetrahydropyridine. *J. Biol. Chem.* **1992**, *267*, 23601−23608.
(29) Harbour, J. R.; Hair, M. L. Detection of superoxide ions in nonaqueous media. Generation by photolysis of pigment dispersions. *J. Phys. Chem.* **1978**, *82*, 1397−1399.
(30) Roberts, J. L.; Sawyer, D. T. Facile degradation by superoxide ion of carbon tetrachloride, chloroform, methylene chloride, and p,p'-DDT in aprotic media. *J. Am. Chem. Soc.* **1981**, *103*, 712−714.
(31) Schmidt, R.; Tanielian, C.; Dunsbach, R.; Wolff, C. Phenalone, a universal reference compound for the determination of quantum yields of singlet oxygen $O_2(^1\Delta_g)$ sensitization. *J. Photochem. Photobiol., A* **1994**, *79*, 11−17.
(32) Ogunsipe, A.; Maree, D.; Nyokong, T. Solvent effects on the photochemical and fluorescence properties of zing phthalocyanine derivatives. *J. Mol. Struct.* **2003**, *650*, 131−140.
(33) Borah, P.; Sreejith, S.; Anees, P.; Menon, N. V.; Kang, Y.; Ajayaghosh, A.; Zhao, Y. Near-IR squaraine dye-loaded gated periodic mesoporous organosilica for photo-oxidation of phenol in a continuous-flow device. *Sci. Adv.* **2015**, *1*, No. e1500390.
(34) Wasserman, H. H.; Larsen, D. L. Formation of 1,4-endoperoxides from the dye-sensitized photo-oxygenation of alkylnaphthalenes. *J. Chem. Soc., Chem. Commun.* **1972**, *5*, 253−254.
(35) Wasserman, H. H.; Wiberg, K. B.; Larsen, D. L.; Parr, J. Photooxidation of methylnaphthalenes. *J. Org. Chem.* **2005**, *70*, 105−109.
(36) Turro, N. J.; Chow, M.-F. Mechanism of thermolysis of endoperoxides of aromatic compounds. Activation parameters, magnetic field, and magnetic isotope effects. *J. Am. Chem. Soc.* **1981**, *103*, 7218−7224.
(37) Wu, H.; Song, Q.; Ran, G.; Lu, X.; Xu, B. Recent developments in the detection of singlet oxygen with molecular spectroscopic methods. *TrAC, Trends Anal. Chem.* **2011**, *30*, 133−141.
(38) Ho, D. G.; Gao, R.; Celaje, J.; Chung, H.-Y.; Selke, M. Phosphadioxirane: A peroxide from an ortho-substituted arylphosphine and singlet dioxygen. *Science* **2003**, *302*, 259−262.
(39) Wilkinson, F.; Helman, W. P.; Ross, A. B. Rate constants for the decay and reactions of the lowest electronically excited singlet state of molecular oxygen in solution. An expanded and revised compilation. *J. Phys. Chem. Ref. Data* **1995**, *24*, 663−1021.
(40) Zhang, D.; Gao, R.; Afzal, S.; Vargas, M.; Sharma, S.; McCurdy, A.; Yousufuddin, M.; Stewart, T.; Bau, R.; Selke, M. Intramolecular arene epoxidation by phosphadioxiranes. *Org. Lett.* **2006**, *8*, 5125−5128.
(41) Gao, R.; Ho, D. G.; Dong, T.; Khuu, D.; Franco, N.; Sezer, O.; Selke, M. Reaction of arylphosphines with singlet oxygen: Intra- vs. intermolecular oxidation. *Org. Lett.* **2001**, *3*, 3719−3722.
(42) Bartusik, D.; Aebisher, D.; Lyons, A. M.; Greer, A. Bacterial inactivation by a singlet oxygen bubbler: Identifying factors controlling the toxicity of $^1O_2$. *Environ. Sci. Technol.* **2012**, *46*, 12098−12104.
(43) Darmanyan, A. P.; Foote, C. S. Solvent effects on singlet oxygen yield from n,π* and π,π* triplet carbonyl compounds. *J. Phys. Chem.* **1993**, *97*, 5032−5035.
(44) Lacombe, S.; Cardy, H.; Simon, M.; Khoukh, A.; Soumillion, J. Ph; Ayadim, M. Oxidation of sulfides and disulfides under electron transfer or singlet oxygen photosensitization using soluble or grafted sensitizers. *Photochem. Photobiol. Sci.* **2002**, *1*, 347−354.
(45) Adam, W.; Saha-Moeller, C.; Schoenberger, A.; Berger, M.; Cadet, J. Formation of 7,8-dihydro-8-oxoguanine in the 1,2-dioxetane-induced oxidation of calf thymus DNA: Evidence for photosensitized DNA damage by thermally generated triplet ketones in the dark. *Photochem. Photobiol.* **1995**, *62*, 231−238.
(46) Davidson, R. S.; Bartholomew, R. F. The photosensitized oxidation of amines. Part I. The use of benzophenone as a sensitiser. *J. Chem. Soc. C* **1971**, *12*, 2342−2346.
(47) Bregnhøj, M.; Westberg, M.; Jensen, F.; Ogilby, P. R. Solvent-dependent singlet oxygen lifetimes: Temperature effects implicate tunneling and charge-transfer interactions. *Phys. Chem. Chem. Phys.* **2016**, *18*, 22946−22961.
(48) Chavan, S. A.; Maes, W.; Gevers, L. E. M.; Wahlen, J.; Vankelecom, I. F. J.; Jacobs, P. A.; Dehaen, W.; De Vos, D. E.


DOI: 10.1021/acsomega.9b00831
*ACS Omega* 2019, 4, 8290−8298

Porphyrin-functionalized dendrimers: Synthesis and applications as recyclable photocatalysts in a nanofiltration membrane reactor. *Chem. - Eur. J.* **2005**, *11*, 6754−6762.
(49) Ramamurthy, V. Photochemistry within a water-soluble organic capsule. *Acc. Chem. Res.* **2015**, *48*, 2904−2917.
(50) Chen, Y.-Z.; Wu, L.-Z.; Zhang, L.-P.; Tung, C.-H. Confined space-controlled hydroperoxidation of trisubstituted alkenes adsorbed on pentasil zeolites. *J. Org. Chem.* **2005**, *70*, 4676−4681.
(51) Davies, A. G. The Schenck rearrangement of allylic hydroperoxides. *J. Chem. Res.* **2009**, 533−544.
(52) Dussault, P. H.; Eary, C. T.; Woller, K. R. Total synthesis of the alkoxydioxines (+)- and (-)-chondrillin and (+)- and (-)-plakorin via singlet oxygenation/radical rearrangement. *J. Org. Chem.* **1999**, *64*, 1789−1797.
(53) Bellucci, G.; Chiappe, C.; Marioni, F.; et al. The cytochrome P-450 catalyzed oxidation of 1-methylcyclohexene. Competition between hydroxylation and epoxidation and absolute stereochemistry of the epoxidation. *Bioorg. Med. Chem. Lett.* **1991**, *1*, 121−124.
(54) Peter, S.; Kinne, M.; Ullrich, R.; Kayser, G.; Hofrichter, M. Epoxidation of linear, branched and cyclic alkenes catalyzed by unspecific peroxygenase. *Enzyme Microb. Technol.* **2013**, *52*, 370−376.
(55) Clennan, E. L.; Sram, J. P. Photooxidations in zeolites. Part 2: A new mechanistic model for reaction selectivity in singlet oxygen ene reactions in zeolitic media. *Tetrahedron Lett.* **1999**, *40*, 5275−5278.
(56) Stratakis, M.; Raptis, C.; Sofikiti, N.; Tsangarakis, C.; Kosmas, G.; Zaravinos, I.-P.; Kalaitzakis, D.; Stavroulakis, D.; Baskakis, C.; Stathoulopoulou, A. Intrazeolite photooxygenation of chiral alkenes. Control of facial selectivity by confinement and cation-$\pi$ interactions. *Tetrahedron* **2006**, *62*, 10623−10632.
(57) Robbins, R. J.; Ramamurthy, V. Generation and reactivity of singlet oxygen within zeolites: Remarkable control of hydroperoxidation of alkenes. *Chem. Commun.* **1997**, *11*, 1071−1072.
(58) Singleton, D. A.; Hang, C.; Szymanski, M. J.; Meyer, M. P.; Leach, A. G.; Kuwata, K. T.; Chen, J. S.; Greer, A.; Foote, C. S.; Houk, K. N. Mechanism of ene reactions of singlet oxygen. A two-step no-intermediate mechanism. *J. Am. Chem. Soc.* **2003**, *125*, 1328−1319.



DOI: 10.1021/acsomega.9b00831
*ACS Omega* 2019, 4, 8290−8298